Research Article | Vol. 9, No. 11 | 1 Nov 2018 | BIOMEDICAL OPTICS EXPRESS 5280
Biomedical Optics EXPRESS

Phase-stability optimization of swept-source optical coherence tomography

SUCBEI MOON[1,2] AND ZHONGPING CHEN[1,3,*]

[1]Beckman Laser Institute, University of California, Irvine, Irvine, CA 92617, USA
[2]Department of Physics, Kookmin University, Seoul 02707, South Korea
[3]Department of Biomedical Engineering, University of California, Irvine, Irvine, CA 92697, USA
*z2chen@uci.edu

Abstract: Phase-resolved imaging of swept-source optical coherence tomography (SS-OCT) is subject to phase measurement instabilities involved with the sweep variation of a frequency-swept source. In general, optically generated timing references are utilized to track the variations imposed on OCT signals. But they might not be accurately synchronized due to relative time delays. In this research, we investigated the impact of the signal delays on the timing instabilities and the consequent deviations of the measured phases. We considered two types of timing signals utilized in a popular digitizer operation mode: a sweep trigger from a fiber Bragg grating (FBG) that initiates a series of signal sampling actions clocked by an auxiliary Mach-Zehnder interferometer (MZI) signal. We found that significant instabilities were brought by the relative delays through incoherent timing corrections and timing collisions between the timing references. The best-to-worst ratio of the measured phase errors was higher than 200 while only the signal delays varied. Noise-limited phase stability was achieved with a wide dynamic range of OCT signals above 50 dB in optimized delays. This demonstrated that delay optimization is very effective in phase stabilization of SS-OCT.

1. Introduction

Swept-source optical coherence tomography (SS-OCT) enables depth-resolved interferometric imaging based on frequency-swept light sources. It has a number of attractive features compared to the time-domain OCT (TD-OCT) or spectral-domain OCT (SD-OCT) technologies. It can provide a higher imaging speed in keeping fine resolutions and good sensitivity [1–3]. It can easily work with a balanced photodetector which greatly reduces annoying imaging artifacts coming from common-mode noise components [4,5]. The long-wavelength bands that low-cost silicon image sensors do not support in SD-OCT can be better utilized by SS-OCT for deeper penetration depths in tissue [1]. SS-OCT is also superior in getting long axial ranges of imaging above centimeters [6,7]. Because of those features, SS-OCT has become one of the most promising optical modalities for medical imaging applications.

While conventional OCT imaging takes only intensities of reflection and scattering contrasts, phase information can be taken for secondary imaging contrasts in advanced imaging modalities. Doppler imaging and phase-sensitive OCT angiography techniques are promising OCT derivatives that rely on phase measurement capabilities [8–12]. Sensitive measurement of signal phase can also allow precision elastography [13,14], vibrometry [15], molecular imaging [16,17] and other functional imaging modalities. However, SS-OCT has been regarded less stable in phase measurement than the SD-OCT counterpart because of the inherent instabilities of swept sources. For the case of SD-OCT in contrast, its spectrometer provides a stable detection means by the static operation principle. That explains why SD-OCT has been more popular in applications that require precision phase measurements [9–11] despite its inherent disadvantage of phase washouts [18]. Because of the useful imaging

#341654 https://doi.org/10.1364/BOE.9.005280
Journal © 2018 Received 6 Aug 2018; revised 21 Sep 2018; accepted 25 Sep 2018; published 9 Oct 2018

Biomedical Optics EXPRESS

contrast provided by phase-resolved OCT and the various advantages of SS-OCT modality, demands on phase-stable SS-OCT technology will increase.

Continuously or nearly continuously, a swept source changes its optical frequency of the laser in a sweep. The sweep characteristics are evaluated by a number of factors including the speed, range, implementation cost, sweep linearity and repeatability [19–23]. In most cases, a swept source produces an undesirable nonlinear relation of time to optical frequency and may need OCT signal reassignments for best resolution performance. At the same time, the time-to-frequency relation may exhibit sweep-to-sweep variations which result in uncertainty of frequencies for acquired signals of spectral interferogram. The properties of the inter-sweep variations are subject to the sweeping mechanism. Inside a swept source, the frequency sweep is driven by tunable filtering, cavity-length tuning or chromatic dispersion dynamics. It can be enabled by a mechanical motion [2,6,19], electric current modulation [20,21] or a passive dispersive element [22,23]. For swept sources based on electric tuning or dispersion dynamics, relatively stable operation is expected. But the most widely used types of swept sources have internal mechanical motions and inevitably produce operational instability. For such a swept source, the instable sweep characteristic is one of major sources of phase instability observed in final OCT data.

Several methods have been developed so far to enhance the phase stabilities of SS-OCT systems for given stabilities of swept sources [12,24–29]. In those methods, commonly, a certain optical response of a frequency-domain transfer characteristic is utilized for making a timing reference or a timing control signal. Spectrally encoded by a known signature, time-varying amplitudes of a timing signal obtained from the same swept laser can be compared and correlated to acquired OCT interferograms. The timing mismatches can be corrected or compensated by a hardware or software signal processing means. This can greatly stabilize the phase measurement by assigning or reassigning the acquired interferogram in a properly registered manner. A signal of dual-path interference generated by a Mach-Zehnder interferometer (MZI) or Michelson interferometer is widely used as an excellent timing reference for its fine and periodically sinusoidal property precisely defined in frequency. It is produced by the laser light's passing through an auxiliary interferometer [24,25] or through the OCT interferometer in common signal paths [28]. This sinusoidal interferogram can be analyzed by zero-crossing points known as signal edges [24], Hilbert transformation [26] or an equivalent processing scheme [27]. As an alternative spectral signature, an optical filter with a sharp spectrum can be utilized for a timing reference. A fiber Bragg grating (FBG) is a popular fiber-type device used for that purpose [18,29]. Unlike the case of an MZI interferogram, this provides a single-shot pulse in a sweep which signifies a certain spectral point. In a synchronized operation, those timing signals can be used for an acquisition trigger or a sampling clock fed to the analog-to-digital conversion (ADC) electronics [18,24]. In other ways, an analog waveform of a timing reference can be acquired separately by a secondary channel of the digitizer [25–27] or together with the OCT interferogram by the same ADC channel [28].

In principle, use of timing reference signals must effectively eliminate the timing errors that originate from a swept source if they are properly produced, delivered and processed. In previous studies, many have focused on the production and processing aspects of the timing information. But delivery of a timing signal may also play an important role in stabilization. One thing worth considering is the fact that the timing signal can be temporally delayed in delivery with respect to the OCT interferogram. Then, timing skews can be produced in conjunction to the laser's intrinsic sweep variations. Note that the light signal can be largely delayed by an OCT interferometer which typically ranges in tens of nanoseconds. In addition, there are chances of electric delays involved with cables, passive or active components in all the signal paths. Timing mismatch between the OCT interferogram and the timing signal seems very common. This can induce improper compensation of timing variations and may

Biomedical Optics EXPRESS

degrade the phase stability performance. No one has systematically investigated this effect to the best of our knowledge.

In this research, we studied the impact of signal timing mismatches on phase measurements of SS-OCT in a typical configuration of signal acquisition instrumentation. Particularly, we tested a frequency-swept laser of a popular type which is based on micro-electro-mechanical-system (MEMS) technology [6,7]: a MEMS vertical-cavity surface emitting laser (MEMS-VCSEL) which runs at a high sweep rate of 200 kHz. In experiments, we utilized the electrical timing signals that the MEMS-VCSEL directly provided for timing controls. We accurately quantified excessive timing jitters and the consequent random errors in phase measurement. They were evaluated with different relative delays of the OCT signal and the timing control signals. We found remarkable effects of delay mismatches on the stability performance. To our surprise, a ratio of the best stability obtained to the worst one was more than 200 in terms of phase measurement precision. Stability improvements in two orders of magnitudes were accomplished simply by optimizing the fiber or cable lengths in the test system. It is worth noting that the power of our optimization method was obtained just by delay adjustments without any added complexity to the system configurations. Our observations verified that optimization of signal delays is one of the significant factors for properly utilizing the timing signals for phase-stable SS-OCT operation.

2. Background and theory

In this study, we took advantage of two types of timing reference signals available directly from the swept source. They needed in-depth analysis to find the mechanisms of potential failures. In this section, the nature of the timing signals is described. The properties of phase instability and timing jitters are theoretically analyzed to find how they are related and how they can be properly quantified in relative signal delays.

2.1 k-clocked sampling and λ-triggered acquisition

There may be a large variety of system configurations in an SS-OCT system, not only for the optical part but also on the side of signal acquisition instrumentation. In this study, we chose one of the most widely used configurations: use of an MZI *k*-clock and a sweep trigger signal for the sampling clock and the acquisition trigger, respectively. The MZI *k*-clock is a timing control signal which is produced by an auxiliary MZI from the swept laser [24]. Using the signal edges of the *k*-clock signal, uniform-in-*k* or equal wavenumber-spaced points are defined in time. Sampling the OCT interferogram at the edges automatically corrects the nonlinear sweep characteristic because the edge timing is registered effectively in the *k* domain. At the same time, the sampling operation is stabilized even in the presence of inter-sweep variations. A signal from a Fabry-Perot filter can play the same role of the *k*-clock [8]. Most commercially available frequency-swept sources currently equip internal MZIs for *k*-clock generators.

Along with the *k*-clocked sampling technique, *triggered acquisition* is a popular mode of the digitizer operation. Produced in synchronization with the laser's sweeping action, a sweep trigger signal can be used to determine a start time of the digitizer's sampling operation in the triggered acquisition mode. Once triggered, the digitizer acquires a preassigned number of signal samples in a time series. The laser's internal sweep driving signal or converted optical intensity of the laser output can be used for the purpose of sweep triggers. An optically generated trigger signal from an optical band-pass filter, such as an FBG, can be better suited for the purpose [2,18]. This timing signal can be called *λ-trigger* because its trigger action is aligned by the laser output's passing through a certain wavelength point. By the acquisition mode triggered by the λ-trigger and clocked by the *k*-clock, a high throughput of OCT data processing is realized without signal reassignments. For this convenience, some of commercially available swept sources provide built-in λ-trigger functions for better implementation of triggered acquisition. If not directly available from a source, one can

Biomedical Optics EXPRESS

construct a λ-trigger generator with a tap-out fiber coupler and a band-pass filter of sharp edges with ease. Notice that those two types of timing references are complementary. While the periodic *k*-clock signal provides precisely determined relative timing as a local clock, the λ-trigger gives an absolute timing of a certain spectral event as a global clock. The λ-triggered acquisition in *k*-clocked sampling is a very useful technique even with an extremely stable swept source, and in an OCT system with no phase-sensing requirement. The signal acquisition and processing stages are greatly simplified by them.

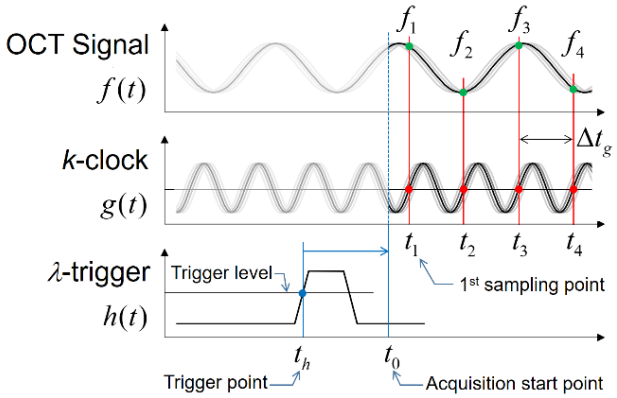

Fig. 1. Schematic timing chart of the acquisition operation with OCT light, *k*-clock and λ-trigger signals. The OCT signal is sampled synchronously at the *k*-clock edges while the first edge was determined by the trigger event of the λ-trigger.

Careful definitions of signal times are required in describing OCT signal and timing control signals. Figure 1 shows a schematic timing chart of three signals to be considered: OCT interferogram, *k*-clock and λ-trigger signals. They are denoted by $f(t)$, $g(t)$ and $h(t)$, respectively, as functions of time t. Throughout this report, signal edges are represented by rising edges of positive slopes for simplicity without loss of generality. The λ-trigger signal is assumed to be a rectangular pulse after being discriminated by a certain intensity level. Indeed, a sweep trigger signal of any type can be used instead of a λ-trigger if it is stable enough in timing.

In the triggered acquisition mode of the digitizer operation, the edge of a λ-trigger initiates a series of signal samplings at the edge time of t_h. It usually takes a constant time delay in nanoseconds for the actual acquisition start point, t_0, due to the processing time of the ADC electronics. The acquisition start point of t_0 is followed by sampling points of the *k*-clock edges, t_n for a positive integer n where the ADC is clocked. The digitizer measures the voltage level of the converted OCT signal in sampling. The acquired digital information is a time series of signals quantized at voltage level. A first sampling point, t_1, is always found after t_0 by this operation mode. In Fig. 1, a clock-to-sample delay in the digitizer is neglected for simplicity.

2.2 Types of delay-sensitive timing deviations

The sweep instability of a laser produces timing uncertainties for the three signals. The intervals between adjacent sampling times (t_n and t_{n+1} for any n) may fluctuate because of the local variation of the laser's sweep speed. The average period is Δt_g which is the inverse of the average *k*-clock frequency. The local deviations of Δt_g are intended to track the laser's sweep in variation. The timing jitters of the OCT signals are compensated in acquisition by this way. Nevertheless, the time fluctuation of t_1 with respect to t_0 must be zero when the two timing control signals are perfectly correlated. In reality, there can be considerable inconsistencies of the *k*-clock timing to both the OCT interferogram and the λ-trigger timings.

Biomedical Optics EXPRESS

Two different types of timing inconsistency problems are considered here: timing instability of OCT signal to *k*-clock (*f*-*g* timing deviation) and *k*-clock to λ-trigger (*g*-*h* timing deviation). Naturally, the *k*-clock only gives correct timing to the light signal part which produced the *k*-clock. In the presence of random fluctuations in sweep speed, correlation of the *k*-clock signal to the OCT interferogram would decrease if they were in a relative time delay caused by different signal paths. The loss of timing correlation can be quantified by the random timing deviations of $f(t)$ in respect to the edge times of t_n. They can be measured by the time-domain fluctuations of a certain signal point when the OCT signal can be assumed to be non-varying in multiple sweeps. A zero-crossing point of a sinusoidal interferogram can be a good point for examination.

The same timing analysis can be applied to the *g*-*h* timing deviation. However, there is one more factor to be considered. In the triggered acquisition, the only purpose of λ-triggering is to stably determine a first sampling point t_1 in a varying sweep. The *g*-*h* timing deviation makes no difference unless it alters an edge for t_1 from sweep to sweep. Alternation of t_1-edges is not only affected by the timing jitters but also depends on the average temporal relation of the λ-trigger's edge to an array of *k*-clock edges. For a given random timing deviation, frequent alternations will occur when the acquisition start point t_0 temporally collides with one of the *k*-clock edges. In the *edge collision*, the average position of the λ-trigger's effective edge (t_0) coincides with a *k*-clock's edge within a probable level of random deviations. It can make the ADC instrument occasionally miss the *k*-clock edge in the closest neighborhood so that it gets clocked by the next one with a large timing jump. Figure 2(a) describes this edge collision effect. The edge of t_1 is not stably determined but randomly alternates in the edge collision. A minute *g*-*h* timing deviation is magnified to a timing jump as large as the clock period of Δt_g. This edge collision problem can be alleviated by placing t_0 well between two *k*-clock edges with sufficient temporal margins given to the relative delays. This is achieved by fine delay tunings performed precisely in temporal fractions of Δt_g. This optimization effort is only effective when a probable *g*-*h* timing deviation is surely lower than a half of Δt_g.

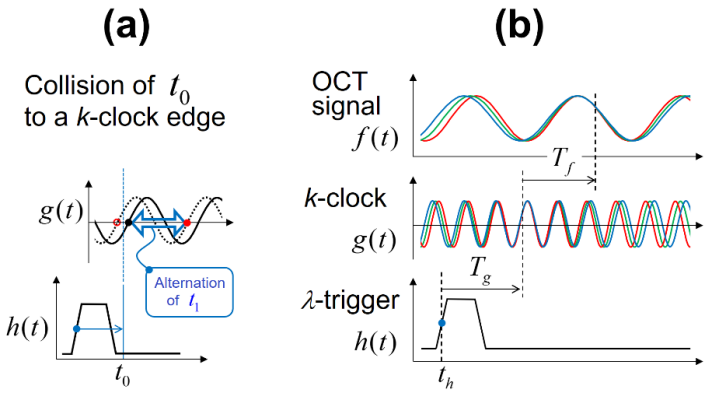

Fig. 2. Mechanism of the edge collision effect (a) and the definition of relative time delays between the signals (b), graphically described in timing charts.

In this report, we define two relative time delays, T_f as the relative time delay of the OCT signal to the *k*-clock signal and T_g as that of the *k*-clock to the λ-trigger signal, respectively. Figure 2(b) shows the illustrative definitions of the time delays in a timing chart. In a system, the relative delays of those signals are produced by optical or electric signal propagations. Passive elements like optical fibers and electric coaxial cables produce dominant portions of total delays. They hardly exhibit short-term fluctuations but give constant delays. Their signal propagation speeds are approximately 2×10^8 m/s or 20 cm/ns for standard single-mode fibers such as SMF-28 and 50-Ω coaxial cables such as RG-58. Compensation of signal

Biomedical Optics EXPRESS

delays can be realized by inserting delay cables, either optical or electrical, in the middle of the signal path. The effect of the time delays should be investigated in a quantitative manner to find the optimum point.

2.3 Timing jitters and phase deviation

The precision performance of phase measurement is affected by several factors including the signal-to-noise ratio (SNR) and the timing jitters of signal acquisition instruments. In a native signal form, the stability can be evaluated by random timing deviation. For a sampled signal of a frequency component, the total amount of timing deviation, σ_{total}, is obtained from a sum of squares with an SNR-involved deviation (σ_{SNR}), optics-induced deviation (σ_{opt}) and an electric timing jitter (σ_{elec}) as

$$\sigma_{total} = \sqrt{\left(\sigma_{SNR}\right)^2 + \left(\sigma_{elec}\right)^2 + \left(\sigma_{opt}\right)^2} \tag{1}$$

measured all in standard deviation. Here, σ_{SNR} is a product of the random noises that reside at the signal frequency. Independently of the system, it gives the fundamental limit of phase measurement [30,31]. If the SNR is dominantly determined by the optical shot noise, σ_{SNR} can be interpreted as the shot noise-limited deviation. Meanwhile, σ_{opt} is from fluctuations of the optical path-length difference (OPD) of the sample and reference arms. It is usually slowly varying but may include high-frequency vibrations which can affect the phase measurement. Finally, σ_{elec} is a collective timing skew of electric signals that mainly occur in the ADC electronics. It is a systematic factor independent of the acquired OCT signal. We neglect σ_{opt} because it mostly appears as an environmental factor. In the total deviation, σ_{SNR} becomes dominant for a low-SNR signal while σ_{elec} can solely determine the total deviation for a very high-SNR signal.

The electric timing jitter of σ_{elec} is a time-domain random error. A common source of σ_{elec} is the intrinsic timing jitter of the ADC device. Failures of the k-clocked operation due to signal delays may contribute to this. In SS-OCT, the time of signal sampling corresponds to an optical frequency or, equivalently, a point in wavenumber k in the laser bandwidth. Thus, the time deviation of δt involved with σ_{elec} is converted to a wavenumber deviation, δk. The acquired spectral signal is transformed to a reflectance profile of an A-line presented in the domain of halved OPD denoted by z. In a conceptually simple case of global time deviations, a signal shift in k is equally applied to the entire A-line data set. By the properties of Fourier transform, the signal translation in k is transformed to z-dependent phase shifts of $\delta k \cdot (2z)$. It is the very case of edge collision caused by a flawed λ-trigger action. In a collision, an occasional jump of t_1 point produces a shift of $\Delta n = \pm 1$ for data, f_n. In an average sense, a relation of $k = 2\pi/\lambda_c$ is taken for a center wavelength λ_c. A deviation of δk can be approximated to $-2\pi/\lambda_c^2 \cdot \delta\lambda$ for a wavelength deviation $\delta\lambda$. Neglecting the sign, the phase deviation $\delta\phi$ can be expressed by

$$\delta\phi = \delta k \cdot (2z) \approx \left(\frac{4\pi\gamma \cdot \delta t}{\lambda_c^2}\right) \cdot z \tag{2}$$

where γ is the sweep rate of wavelength per time. Therefore, the effect of edge collisions is more intense for signal components of a larger z. Equation (2) can be generalized to non-global timing jitters. For local random timing deviations, an effectively weighted sum of all the timing errors that occur in data points should be taken for δt. By randomness, δt is reduced from a jitter of individual points by a certain factor. In general, electric jitter-induced phase deviation can be expressed by $\delta\phi = \alpha \cdot z$ with a *phase-stability decline coefficient*, α. It gives a normalized measure of how unstable a system is in its signal acquisitions involved with electric timing jitters.

Biomedical Optics EXPRESS

In conjunction to the inter-sweep variation of sweep rate γ, a relative delay of OCT signals to the k-clock contributes to electric timing jitters. Here, the role of a k-clock can be interpreted as measuring the k-domain sweep rate of $\gamma' \equiv (dk/dt) = (-2\pi/\lambda^2)\cdot\gamma$ at a certain temporal point t. Suppose that the k-clock is undesirably delayed by Δt. Then, the timing information of γ' obtained from the signal at t will be used for sampling the signal at $\{t + \Delta t\}$. Consequently, k will be misread with an offset of Δk. The offset is proportional to the delay by $\Delta k = \gamma' \Delta t$ when a constant sweep rate is assumed over the interval for small Δt. If the sweep rate gets changed slightly by $\delta\gamma'$ in another sweep, the very point with the offset of Δk will be shifted in t. This shift will be equal to a timing deviation of a sampling point around the point. Denoting the resulting timing deviation with δt, this gives a relation of $\Delta k = (\gamma' + \delta\gamma')\cdot(\Delta t - \delta t)$ for the same point of the offset Δk. Still, $\Delta k = \gamma' \Delta t$ holds together. Combining those relations gives

$$\chi \equiv \frac{\delta t}{\Delta t} \approx \frac{\delta\gamma'}{\gamma'} = \frac{\delta\gamma}{\gamma} \tag{3}$$

in a first-order approximation for small $\delta\gamma'$. Thus, the normalized timing deviation, χ, equals the normalized deviation of sweep rate. For a given instability of constant χ, the timing deviation is proportional to the signal's relative delay in a linear relation of $\delta t = \chi\cdot\Delta t$ by Eq. (3).

2.4 SNR-limited phase deviation

The SNR-limited phase deviation has a different property from that of the electric timing jitters. The random noise added to the OCT signal also has a phase in the Fourier analysis. This gives the nature of the SNR-limited phase deviations. The SNR-involved phase error is derived from a statistical signal analysis. A signal at a point of the Fourier-transformed domain is expressed by $s = a_s\cdot\exp(\mathrm{i}\phi_s)$ with a real signal amplitude of a_s and a signal phase of ϕ_s. A random noise at the same point is a complex random variable of $N = \{N_r + \mathrm{i}N_i\}$ with real part N_r and imaginary part N_i. The random noise has a uniform distribution on phase so that N_r and N_i are not correlated. The noise power is the squared absolute value of noise N which is expressed by $|N|^2 = \{N_r^2 + N_i^2\}$ which is still random. The mean of the noise power is significant which is obtained by $\langle|N|^2\rangle = \langle N_r^2\rangle + \langle N_i^2\rangle$. Here, the expectation value or the mean of multiple measurements is denoted by $\langle X\rangle$ for a random variable X. Due to the random-phase property of N, the mean noise power $\langle|N|^2\rangle$ turns out to be $2\cdot\langle N_r^2\rangle$ or $2\cdot\langle N_i^2\rangle$. The SNR of signal-to-noise power ratio is expressed by

$$SNR \equiv \frac{|s|^2}{\left\langle |N|^2 \right\rangle} = \frac{a_s^2}{2\left\langle N_i^2 \right\rangle} \tag{4}$$

for the signal s and the noise N.

The acquired signal of $\{s + N\}$ has its phase different from that of s. The phase is an angular measurement expressed by $\Phi = \arg\{s + N\}$. Hence, the phase error of the acquired signal $\{s + N\}$ is obtained by angular difference of $[\arg\{s + N\} - \arg\{s\}]$. For simplicity, let us pick a special case of $N = a_s$ at $\phi_s = 0$ without loss of generality. Then, the phase error simply equals $\arg\{s + N\}$ because $\arg\{s\} = 0$ is given for the case. For a high SNR where s is far more intense than N, the random phase error $\delta\Phi$ can be approximated to

$$\begin{aligned} \delta\Phi &= \arg\{s + N\} = \arg\{(a_s + N_r) + \mathrm{i}N_i\} \\ &= \arctan\left(\frac{N_i}{a_s + N_r}\right) \approx \frac{N_i}{a_s + N_r} \xrightarrow{(a_s \gg N_r)} \frac{N_i}{a_s} \end{aligned} \tag{5}$$

Biomedical Optics EXPRESS

by the property of arctan $X \approx X$ for small X.

The variance of the squared standard deviation will be denoted by $\sigma^2[X]$ for a random variable X. It is formally defined by $\sigma^2[X] = \langle (X - \langle X \rangle)^2 \rangle$. Here, $\langle \delta\Phi \rangle = 0$ automatically holds by the random phase. The variance of $\delta\Phi$ is obtained by taking $\sigma^2[\delta\Phi] = \langle \delta\Phi^2 \rangle$ as

$$\sigma^2\left[\delta\Phi\right] = \frac{\left\langle N_i^2 \right\rangle}{a_s^2} \tag{6}$$

from the relation of $\delta\Phi = N_i/a_s$ given by Eq. (5). This can be expressed with *SNR* by using Eq. (4). The standard deviation of the phase error caused by a finite *SNR*, $\delta\phi_{SNR}$, is found by

$$\delta\phi_{SNR} \equiv \sqrt{\sigma^2\left[\delta\Phi\right]} = \frac{1}{\sqrt{2 \cdot SNR}} \tag{7}$$

for phase in radian. If one takes the difference of two phase measurements, the variance will be doubled and the standard deviation will simply be $(SNR)^{-1/2}$ [28,30,31]. For example, if the *SNR* is 20 dB (= 10^2) for a signal, $\delta\phi_{SNR}$ will be 0.071 radian in a single-shot measurement while the differential phase measurement will approximately give 0.10 radian. The SNR-limited phase deviation only depends on the SNR level and must appear constant in z.

3. Experiment and result

3.1 Test setup and method

A MEMS-VCSEL swept source (SL1310V1-20048, Thorlabs Inc.) was used as a light source in our experiment. It is one of the fastest models commercially available which sweeps 200,000 times per second. The optical bandwidth was 100 nm centered at 1.3 μm in wavelength. Its internal MZI provided a *k*-clock signal of ~1.0 GHz by the internal OPD of 48 mm for a long imaging range. The utilizable part of the sweep was 3 μs in duration and made an average sweep rate of 3×10^{-5} μm/ns. The source also provided an FBG-based λ-trigger signal output. However, its λ-trigger signal contained secondary pulses at the returning sweeps which were shorter in duration. To remove the unwanted pulse part from the λ-trigger, we utilized a simple home-made electric circuit of a *pulse picker*. It exclusively picked up the main pulses of longer durations based on a low-pass filter and a comparator. In this way, the λ-trigger signal was conditioned to give a single rising edge per sweep. It could be used to determine the acquisition start time by the edge trigger. Our pulse picker circuit produced a signal delay of 41 ns including cable delays.

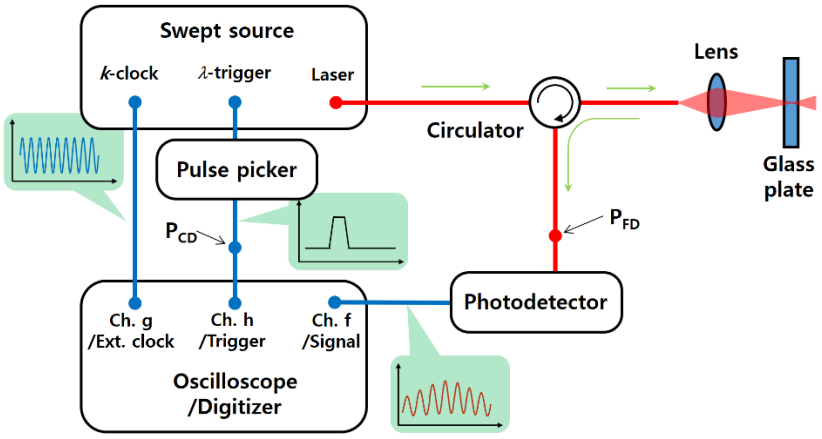

Fig. 3. Schematic diagram of test setup in a common-path interferometer configuration.

Biomedical Optics EXPRESS

The test setup was constructed for evaluating the stability performance with the swept source. Figure 3 shows a schematic diagram of our test setup. A simple common-path interferometer was constructed with an optical circulator. A 1.0-mm thick plate of a standard microscope glass slide was placed at the focus of the objective lens. It gave two reflection points at the front and back surfaces producing an autocorrelation interference. Use of common-path optics has several advantages. The interferogram generated by a sample's autocorrelation is very stable over a long period of time. No polarization and chromatic dispersion-involved effects complicate the test conditions [32]. In our test setup, a high-speed photodetector converted the optical interferogram to an electric signal form. A high-speed multi-channel oscilloscope (MSO54, Tektronix Inc.) was utilized for signal acquisition means. It acquired three signals of OCT interferogram, *k*-clock and λ-trigger signals simultaneously at a high sampling rate of 12.5 GS/s. The oscilloscope was run by its internal sampling clock. Three coaxial cables used for electric signal delivery had equal lengths in our test setup.

In our oscilloscope-based test, the effect of different signal delays was investigated by digitally shifting the acquired signals in a post-processing stage. The *k*-clocked λ-triggered operation was simulated in the digital signal processing. In timing analysis, signal edges were searched in high precision by linear interpolations. For the OCT interferogram, zero-crossing points were considered. The interferogram signal was processed by a digital high-pass filter in order for the DC component to be removed. The relative fluctuations of timing could be measured for those three signals. The statistical deviations were quantified at the same edges with a number of sweeps.

Later, stability evaluations were repeated by replacing the oscilloscope with a high-speed digitizer in an actual SS-OCT operation mode. We used a signal digitizer which is popular for SS-OCT instrumentation (ATS9360, Alazartech Inc.). It can operate at <1.8 GS/s with a 12-bit digitizing depth. In our digitizer-based test, the *k*-clock signal was fed to the digitizer for an external sampling clock. The λ-trigger signal was used as an acquisition trigger in the triggered acquisition mode. The digitizer was set to sense rising edges in all cases. The actual sampling rate was ~1 GS/s by the *k*-clock frequency. The axial range of A-lines was 12 mm in air. In this test, delay adjustments were physically made with actual cables. An optical fiber delay was applied to the OCT signal at a point indicated by P_{FD} in Fig. 3. This fiber delay could adjust T_f in the system. A coaxial cable delay was applied to the λ-trigger signal at a point indicated by P_{CD} in Fig. 3. It could adjust T_g. Again, the time-domain stability of the acquired interferogram signal was evaluated at zero-crossing points. For finer temporal resolutions, the interferogram data were partially reconstructed by cubic interpolations around a zero-crossing point of interest with a data point interval of ~2 ps.

3.2 Result of oscilloscope-based test

Two types of timing stabilities were evaluated from the oscilloscope-based test: *g*-*h* deviations and *f*-*g* deviations, respectively. In evaluation of the *g*-*h* deviations, the *k*-clock signal, $g(t)$, was temporally shifted by a delay compensation of ΔT_g with respect to the λ-trigger signal, $h(t)$. When the delays were matched by $T_g = \Delta T_g$, the best timing stability was expected. A rising edge of the *k*-clock signal was chosen in the temporal vicinity of the λ-trigger's edge after a delay compensation was applied digitally. Figure 4 shows the acquired *k*-clock signals at the λ-trigger edges with different levels of delay compensations. A vertical dashed line depicts the edge time of the λ-trigger in each plot. The *k*-clock waveform significantly dithered in time by the random timing jitters. They could be evaluated in standard deviation with data of 900 consecutive sweeps. Figure 5(a) shows the result of the timing jitter measurements as a function of ΔT_g. It shows that the timing jitter was at minimum around $\Delta T_g = -50$ ns and increased at both sides. The minimum standard deviation was 81 ps at the best delay compensation.

Biomedical Optics EXPRESS

As observed in Fig. 5(a), the evaluation result clearly demonstrates a significant effect of signal delays on the measured timing correlations. The delay mismatch of T_g = –50 ns found at the minimum deviation is partially explained by the time delay of 41 ns that our pulse picker circuit added to the λ-trigger signal. The trigger's processing time of t_h to t_0 might contribute considerably as well. At first glance, the timing jitters below 100 ps seem low enough in stably determining first sampling points because it is surely shorter than the average sampling interval of Δt_g = 1.02 ns. But it is still too large to neglect the edge collision effect.

For evaluating the *f*-*g* deviations, the timing jitters of the OCT interferogram were evaluated in a similar way. At first, a delay compensation of ΔT_g = –47 ns was set for the best *g*-*h* timing stability. First sampling points were stably determined by the λ-trigger signal with no edge collision effect in account. Then, the effect of delay compensations applied to the interferogram was examined. Figure 5(b) shows the measured timing jitters in varying the delay compensation of ΔT_f by which a relative delay of $f(t)$ to $g(t)$ was adjusted. As expected, the best stability was obtained at a certain amount of delay compensation. A jitter of 15.7 ps was obtained at the minimum for ΔT_f = –40 ns. Out of the delay-matched regime, the timing jitter increased nearly linearly with a slope of χ = ± 1.5 ps/ns. In other words, a delay mismatch of every 10 ns produced additional timing deviation of 15 ps in a proportional manner. This result suggests that a meter-level delay adjustment will be required for OCT signals or *k*-clock signals in order to obtain the best stability performance.

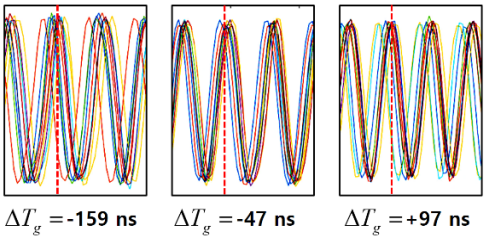

Fig. 4. Traces of the acquired *k*-clock signals at λ-trigger edges for different delay compensations. Fifteen traces are overlaid in each plot.

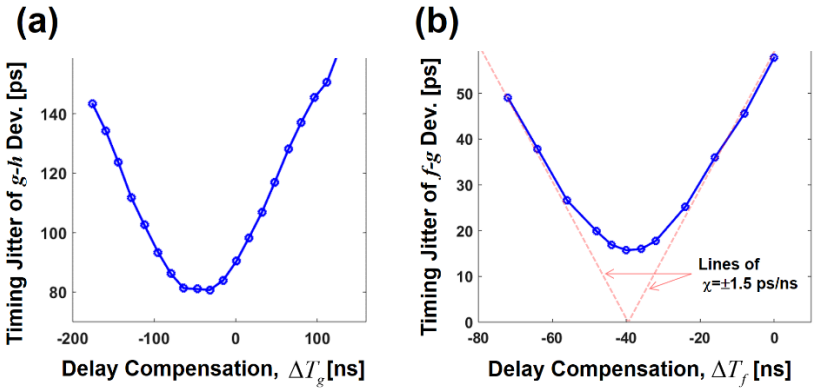

Fig. 5. Timing jitters of the *k*-clock edges to the λ-trigger edges (a), and timing jitters of the interferogram's zero-crossing points to the *k*-clock edges (b), all measured in standard deviation at different delay compensations of ΔT_g and ΔT_f, respectively.

3.3 Result of OCT digitizer-based test

The digitizer-based test was performed by operating an OCT digitizer in a *k*-clocked λ-triggered acquisition mode. This test could demonstrate exact performance which would be obtained in an actual SS-OCT system. The result of the oscilloscope-based test described

Biomedical Optics EXPRESS

above suggested that the delay mismatch of T_g was not so critical by itself. We did not apply a physical delay compensation to T_g for this reason. So, a random timing jitter of ~90 ps in the *g*-*h* deviation was accepted in this digitizer-based test. But a fine delay tuning of a small quantity was still necessary to avoid possible edge collisions. A handful of short coaxial cables with length differences of a few centimeters were prepared. Their delay differences were carefully measured with a signal generator and an oscilloscope. While each was inserted one by one in the cable connection of the λ-trigger, the timing jitters of the interferogram signal were evaluated at zero-crossing points. This timing evaluation was performed at the central part of the interferogram where the amplitude was the highest. Consecutively acquired 1,000 interferograms were examined in the statistical analysis. Notice that this evaluation differs from the case of Fig. 5(a). The stability of the interferogram was evaluated rather than that of the *k*-clock. Also, unlike the case of Fig. 5(a), the edge collision might give an effect because of the triggered operation mode of the digitizer.

In our experiment, a fine delay adjustment on T_g was found to make a critical impact on the measured timing stability. Figure 6(a) shows the timing jitters of the OCT interferogram measured with different delay adjustments ($\Delta T_g'$) in the digitizer-based test. The measured timing jitters varied largely in a manner very sensitive to the applied delay adjustment. This property was explained by the edge collision effect. In the edge collision, first sampling points could alter as widely as the *k*-clock period, Δt_g. The standard deviation would be a half of Δt_g in a case of perfect collisions. Figure 6(a) shows high-jitter regions were repeated in a period that matches Δt_g = 1.02 ns by the cyclic property of the collision. The worst timing jitter nearly matched $\Delta t_g/2$ = 510 ps. Those observations clearly verified the presence of edge collisions. The collision-free regions of low jitters were estimated to be <0.5 ns in full width. Thus, without fine delay tunings, the chance of obtaining a collision-free performance was relatively low below 50%.

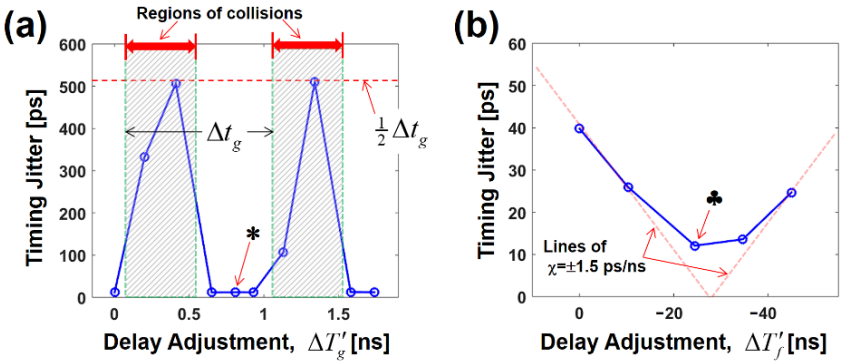

Fig. 6. Timing jitters of the OCT interferogram measured with different delay adjustments of the λ-trigger signal (a) and the OCT signal (b) obtained from the digitizer-based test.

In the next stage, the impact of T_f was examined in the digitizer-based test. In order to prevent the edge collisions, the λ-trigger delay was tuned at the same level as marked by an asterisk (*) in Fig. 6(a). A delay adjustment, $\Delta T_f'$, was made on T_f by an optical fiber inserted before the photodetector. Figure 6(b) shows the measurement result of timing jitters. It exhibited a trend similar to that of Fig. 5(b). The stability performance was best at a certain compensation delay and degraded gradually. The standard deviation was 12.1 ps at the minimum. Again, lines of slope $\chi = \pm$ 1.5 ps/ns well represented the out-of-matching increase in the same way as the plot of Fig. 5(b). An additional signal delay of ~7 ns was made by cable connections in the digitizer-based test so that $\Delta T_f'$ was approximately equal to ΔT_f plus 7 ns. The optimal delay compensations found by the two different tests differed by a few nanoseconds. This small difference could be explained by propagation delays made in different ADC architectures. The only considerable difference between the two results of Fig.

Biomedical Optics EXPRESS

6(b) and Fig. 5(b) was the minimum jitters observed at the best delay matching conditions. They must have largely depended on the ADC performances. The reasons for a better performance in the digitizer case might include its lower quantization noise (12 bits vs. 8 bits in ADC depth) and a better interpolation method applied in the post-processing (cubic vs. linear interpolation). In the digitizer-based test, the delay mismatch was found to make more significant impacts because of the lowered minimum jitters. A mismatch of 10 ns, equivalently a 2-m long cable in excess, could double the timing deviations.

At a delay-matched condition which is marked by ♣ in Fig. 6(b), the acquired interferogram signals were further examined in inter-sweep stability. They were very stable and appeared to be virtually non-varying signals in a sweep-to-sweep comparison. Figure 7 (a) shows the plots of the OCT interferograms in part which were consecutively acquired in the digitizer-based test: 1,000 traces were overlaid in this plot. The inset is a magnified view of a signal cycle in Fig. 7 (a). No noticeable dithering was observed for the signals of remarkable stability. The measured timing jitter (12 ps) was thought to nearly reach the best of the digitizer's inherent timing performance.

The signals were analyzed in the Fourier-transformed domain. Figure 7 (b) shows the OCT A-lines in part obtained by doing fast-Fourier-transform (FFT) on the acquired interferograms. One thousand A-lines were overlaid in this plot. The solid black line laid on the top depicts an averaged A-line by which the noise level was found as arrowed in Fig. 7(b). The average was taken for the powers of the absolutized FFT to be consistent with Eq. (4). In each A-line, two peaks were observed. A high peak was from two of direct surface reflections while a low peak was from an interference of triple reflections to a single reflection made by the front and back surfaces of the glass plate. The difference in OPD, thus, matched the optical thickness of the plate. The two peaks exhibited SNRs of 71.2 dB and 43.5 dB, respectively. The phase stabilities were examined for those two peaks. The high peak produced a standard deviation of phase, $\delta\phi = 8.0 \times 10^{-4}$ radian, while the low peak made $\delta\phi = 4.8 \times 10^{-3}$. Figure 7(c) shows the histograms of the phase deviations measured for the two A-line peaks, respectively. There, the phase deviations were aligned to have their mean at zero. The histograms followed the normal probability distributions of Gaussian functions.

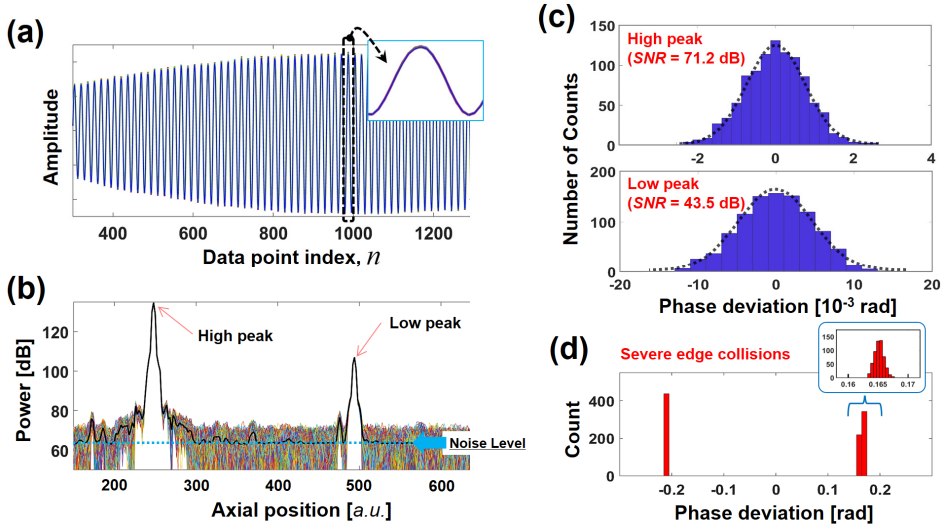

Fig. 7. OCT interferograms consecutively acquired in the digitizer-based test (a), their transformed A-lines (b), the histograms of the measured phases for the two peaks of the A-line data (c), and the histogram of the phase measurements for a case of severe edge collisions (d).

Among various delay combinations, the worst phase stability was obtained from the cases of severe edge collisions. With an optimally matched delay for T_f but in perfect edge

Biomedical Optics EXPRESS

collisions due to badly tuned T_g, the timing jitter could reach ~500 ps in standard deviation as seen in Fig. 6(a) which was expected from the theoretical analysis. Figure 7(d) shows the histogram of measured phases obtained from a case of severe edge collisions for the high peak of *SNR* = 71 dB. The inset histogram is a magnified version of the part at the positive-phase side. The measured standard deviation for the full histogram was 0.19 radian, much larger than the level obtained without collisions. The histogram indicates that the measured phases split into two largely separate groups by the collision effect. Random alternations of first sampling points must have made this effect. Taking only one side of the histogram is equivalent to making a collision-free or collision-compensated situation. The standard deviation dramatically decreased to 7.7×10^{-4} radian, only 0.4×10^{-2} part of the full histogram. After all, the edge collision effect was found to make a tremendous impact on the phase measurements. Phase precisions can fall down by more than two orders of magnitude.

4. Discussion

In this study, we introduced a simple test method of delay-dependent stability evaluations for a swept source and an SS-OCT system. Our oscilloscope-based test provides a convenient way of finding delay mismatches by digitally implemented delays. The digitizer-based test could examine an actual performance of acquisition instrumentation with physical delays. An autocorrelation interference was utilized in our test methods by using a glass plate. No optical perturbation was observed throughout our experiment due to the stable common-path configuration. In an ordinary SS-OCT system, one can perform the same test by blocking the reference arm and unplugging one of two optical inputs to the balanced photodetector.

One more useful feature of our method is that both high-SNR and low-SNR peaks are obtained in an A-line at once. Produced by multiple reflections, a low-SNR peak might give an opportunity to evaluate the SNR-limited performance. A glass plate makes a surface reflectivity of 4% or −14 dB. A triple reflection can make −42 dB or lower. Its SNR will be mostly in the range of 40 to 60 dB which can represent cases of moderate SNR levels. For our digitizer-based test, Eq. (7) gave an estimation of the SNR-limited phase errors. It was calculated to be $\delta\phi = 4.7 \times 10^{-3}$ in theory from the SNR of the low peak, $10^{43.5/10} = 2.2 \times 10^4$. This perfectly agreed with the measured deviation of $\delta\phi = 4.8 \times 10^{-3}$.

Meanwhile, in the case of a high-SNR peak, there was a large difference between the measured deviation ($\delta\phi = 8.0 \times 10^{-4}$) and the SNR limit ($\delta\phi = 1.9 \times 10^{-4}$). This suggests that the electric timing jitter was dominant for such a high-SNR peak (*SNR* = 71 dB). In tissue imaging cases, this level of extreme SNRs is exceptional but can be taken only from specular reflections. Precision measurement of surface displacements can be an exemplary case of such an extreme SNR. Converted to displacement measurements, the obtained phase errors produce length errors of 0.083 nm and 0.50 nm in z for the high-SNR and the low-SNR peaks, respectively.

An objective measure or a figure of merit is required to absolutely quantify the phase measurement precision of a system. Phase stability performances are not well represented by a measured phase error for a certain special case because it depends on the SNR and the axial position. In usual OCT imaging cases, phase-resolved OCT is used to get phase information from in-tissue scatterings at relatively low SNRs. In this context, the system performance can be objectively represented by the range of signals by which nearly SNR-limited performances are obtained. The dynamic range of SNR-limited phase precisions, denoted by $R_{\delta\phi}$, is introduced here. It is defined by the maximum SNR which produces an SNR-limited phase error higher than that of electric jitter-induced phase instability measured for a system. From Eq. (7) and Eq. (2), it is obtained by

$$R_{\delta\phi} = \frac{1}{2 \cdot \delta\phi_{elec}^2} = \frac{1}{2 \cdot (\alpha z)^2} \tag{8}$$

Biomedical Optics EXPRESS

where $\delta\phi_{elec}$ is the phase error involved with σ_{elec}, and α is the phase-stability decline coefficient in a relation of $\delta\phi_{elec} = \alpha \cdot z$. In our digitizer-based test, the electric jitter-induced phase error was estimated to be $\delta\phi_{elec} \approx 8.0 \times 10^{-4}$ from the phase deviation of the high-SNR peak. Then, the dynamic range was estimated to be $R_{\delta\phi} \geq 59$ dB for $z \leq 1.5$ mm. Such a wide dynamic range will exceed most demands in medical OCT imaging. Based on Eq. (7), the phase-stability decline coefficient can be used for an alternative measure of the z-dependent dynamic range. Our test system exhibited $\alpha = 5.3 \times 10^{-4}$ mm^{-1} calculated from Eq. (8). From known α, one can easily find $R_{\delta\phi}$ for any z with Eq. (8). Thus, α can be used for a figure of merit in terms of systematic phase measurement stability. For most applications, $R_{\delta\phi} > 40$ dB may be sufficient for an imaging range of $z < 5$ mm. It approximately requires α to be below 10^{-3} mm^{-1} which can be regarded as a guideline of good phase stability.

We quantitatively evaluated stability degradations involved with delay mismatches as described in Fig. 5(b) and Fig. 6(b). The observed trends agreed well with the theoretical model presented in Eq. (3). In a regime of matched delays, the ADC's intrinsic timing jitter must have been dominant. When the delay was considerably mismatched, the timing deviation proportionally increased at a rate of 1.5 ps/ns. In this *linear degradation* regime, the normalized timing deviation of $\chi \equiv \delta t/\Delta t$ must have made a constant slope. By Eq. (3), the local sweep speed variation of the high-speed MEMS-VCSEL was estimated to be 0.15% in standard deviation. This can be regarded as an objective measure of the sweep instability.

We found the most critical failure related to signal delays was brought by the edge collision effect. While the linear degradation could make timing jitters below 50 ps even for a considerable delay mismatch of 30 ns (6-m cable), the edge collision could give a devastating amount of deviations as large as the ADC sampling period (1.02 ns in ours). Then, the phase instability is directly affected by the average sampling rate of the digitizer in the presence of edge collisions [33]. The phase deviation caused by the edge collision could be estimated by Eq. (2). For the case of Fig. 7 (d), the theoretical prediction gave $\delta\phi = 0.17$ in standard deviation when the conversion parameters were taken for $\gamma = 3 \times 10^{-5}$ μm/ns, $z = 1.5 \times 10^3$ μm, $\delta t = 0.5$ ns and $\lambda_c = 1.3$ μm. This estimation nicely agreed with the measured phase standard deviation of $\delta\phi = 0.19$ radian. The mechanism of the conditional deviation magnification is accompanied by the triggered acquisition operation of the digitizer. Elimination of edge collisions requires careful tuning of T_g with a fine delay precision better than a fraction of the k-clock period (a few centimeters in ours). And it may need careful stability evaluations to find which delay gives a collision-free performance with enough timing margins.

Concerned with the fine delay tuning, we introduce two useful techniques here. First, the delay tuning can be realized by an electrically tunable means. An electric phase shifter is a useful device for this purpose. Alternatively, the λ-trigger's action can be delayed by adjusting the trigger level of the digitizer. For a finite rise time of a λ-trigger signal, increase in the digitizer's trigger level can finely extend the temporal delay without losing any operational stability. Those electric tuning methods are definitely more convenient than physically replacing cables. Second, the edge collision might be easily sensed by using its characteristic property. By nature, it makes homogeneous shifts of data points with an integer Δn for sampled data f_n. For a stable sweep trigger like our λ-trigger signal, the shift of data points can be $\Delta n = \pm 1$ while an instable sweep trigger can make larger shifts of integers. In Choi *et al.*'s method [29], they detected such a global data shift by using a spectral signature made on OCT interferograms. In Song *et al.*'s method [12], a shift in k is detected by phase shifts proportional to z in the transformed domain. Those schemes can be useful in sensing the global data shifts brought by the edge collisions. It is worth noting active electronic components may exhibit temperature dependence in internal propagation delay. Warming up the instruments may help in timing-sensitive systems. In our experiment, we ran the swept source and the digitizer for ten minutes or longer before performing the tests. We observed

Biomedical Optics EXPRESS

timing characteristics varied significantly without such warming-ups. This temperature-related concern necessitates developing a smarter way of adaptive delay tuning for practical systems. If edge collisions are sensed, the OCT system can re-adjust the delay in a closed-loop operation. Such an adaptive delay tuning will eliminate the chance of edge collisions in spite of systematic long-term variations of signal delays.

5. Conclusion

In this research, relative time delays between OCT signal and timing reference signals were considered as potential sources of phase instabilities in a phase-resolved SS-OCT system. Using a popular operation mode of an OCT digitizer, an MZI-based *k*-clock signal and an FBG-based λ-trigger signal were utilized for the ADC sampling clock and for the acquisition trigger, respectively. By experimental tests performed with a high-speed oscilloscope and an OCT digitizer, various aspects of stability performances were examined with concern for optimized signal delays. We found very significant impact of relative delays on phase measurements which necessitated optimally compensating or tuning the signal delays. A linear degradation of phase stability was observed that every nanosecond of delay mismatches produced a timing jitter of 1.5 ps in addition. We also found that a relatively low timing jitter of ~100 ps could be magnified in the process of edge collisions by a triggered acquisition operation. More than two orders of magnitudes could be saved in systematic timing jitters by properly adjusting the signal delays. Through careful optimizations, we obtained an SNR-limited precision performance of phase measurement in a wide dynamic range of SNR over 59 dB at an axial point of $z \leq 1.5$ mm. Our study successfully demonstrated that a phase stabilization technique may require elaborations in signal delivery. We believe our findings will provide a useful guide in developing and managing phase-resolved SS-OCT systems.

Funding

National Institutes of Health (NIH) (P41EB-015890, R01EY-021529, R01EY-026091, R01HL-125084, R01HL-127271, R01EY-028662).

Disclosures

The authors declare that there are no conflicts of interest related to this article.

References

1. J. F. de Boer, R. Leitgeb, and M. Wojtkowski, "Twenty-five years of optical coherence tomography: the paradigm shift in sensitivity and speed provided by Fourier domain OCT [Invited]," Biomed. Opt. Express **8**(7), 3248–3280 (2017).
2. S. Yun, G. Tearney, J. de Boer, N. Iftimia, and B. Bouma, "High-speed optical frequency-domain imaging," Opt. Express **11**(22), 2953–2963 (2003).
3. M. Choma, M. Sarunic, C. Yang, and J. Izatt, "Sensitivity advantage of swept source and Fourier domain optical coherence tomography," Opt. Express **11**(18), 2183–2189 (2003).
4. A. G. Podoleanu, "Unbalanced versus balanced operation in an optical coherence tomography system," Appl. Opt. **39**(1), 173–182 (2000).
5. S. Moon and D. Y. Kim, "Normalization detection scheme for high-speed optical frequency-domain imaging and reflectometry," Opt. Express **15**(23), 15129–15146 (2007).
6. Z. Wang, B. Potsaid, L. Chen, C. Doerr, H.-C. Lee, T. Nielson, V. Jayaraman, A. E. Cable, E. Swanson, and J. G. Fujimoto, "Cubic meter volume optical coherence tomography," Optica **3**(12), 1496–1503 (2016).
7. I. Grulkowski, J. J. Liu, B. Potsaid, V. Jayaraman, C. D. Lu, J. Jiang, A. E. Cable, J. S. Duker, and J. G. Fujimoto, "Retinal, anterior segment and full eye imaging using ultrahigh speed swept source OCT with vertical-cavity surface emitting lasers," Biomed. Opt. Express **3**(11), 2733–2751 (2012).
8. J. Zhang and Z. Chen, "In vivo blood flow imaging by a swept laser source based Fourier domain optical Doppler tomography," Opt. Express **13**(19), 7449–7457 (2005).
9. S. Makita, Y. Hong, M. Yamanari, T. Yatagai, and Y. Yasuno, "Optical coherence angiography," Opt. Express **14**(17), 7821–7840 (2006).
10. L. An, J. Qin, and R. K. Wang, "Ultrahigh sensitive optical microangiography for in vivo imaging of microcirculations within human skin tissue beds," Opt. Express **18**(8), 8220–8228 (2010).

Biomedical Optics EXPRESS

11. J. Fingler, D. Schwartz, C. Yang, and S. E. Fraser, "Mobility and transverse flow visualization using phase variance contrast with spectral domain optical coherence tomography," Opt. Express **15**(20), 12636–12653 (2007).
12. S. Song, J. Xu, S. Men, T. T. Shen, and R. K. Wang, "Robust numerical phase stabilization for long-range swept-source optical coherence tomography," J. Biophotonics **10**(11), 1398–1410 (2017).
13. J. Zhu, Y. Qu, T. Ma, R. Li, Y. Du, S. Huang, K. K. Shung, Q. Zhou, and Z. Chen, "Imaging and characterizing shear wave and shear modulus under orthogonal acoustic radiation force excitation using OCT Doppler variance method," Opt. Lett. **40**(9), 2099–2102 (2015).
14. M. Singh, C. Wu, C.-H. Liu, J. Li, A. Schill, A. Nair, and K. V. Larin, "Phase-sensitive optical coherence elastography at 1.5 million A-Lines per second," Opt. Lett. **40**(11), 2588–2591 (2015).
15. S. Kim, P. D. Raphael, J. S. Oghalai, and B. E. Applegate, "High-speed spectral calibration by complex FIR filter in phase-sensitive optical coherence tomography," Biomed. Opt. Express **7**(4), 1430–1444 (2016).
16. A. Oldenburg, F. Toublan, K. Suslick, A. Wei, and S. Boppart, "Magnetomotive contrast for in vivo optical coherence tomography," Opt. Express **13**(17), 6597–6614 (2005).
17. S. Makita and Y. Yasuno, "Detection of local tissue alteration during retinal laser photocoagulation of *ex vivo* porcine eyes using phase-resolved optical coherence tomography," Biomed. Opt. Express **8**(6), 3067–3080 (2017).
18. H. C. Hendargo, R. P. McNabb, A.-H. Dhalla, N. Shepherd, and J. A. Izatt, "Doppler velocity detection limitations in spectrometer-based versus swept-source optical coherence tomography," Biomed. Opt. Express **2**(8), 2175–2188 (2011).
19. C. M. Eigenwillig, B. R. Biedermann, G. Palte, and R. Huber, "K-space linear Fourier domain mode locked laser and applications for optical coherence tomography," Opt. Express **16**(12), 8916–8937 (2008).
20. Z. Chen, M. Liu, M. Minneman, L. Ginner, E. Hoover, H. Sattmann, M. Bonesi, W. Drexler, and R. A. Leitgeb, "Phase-stable swept source OCT angiography in human skin using an akinetic source," Biomed. Opt. Express **7**(8), 3032–3048 (2016).
21. S. Moon and E. S. Choi, "VCSEL-based swept source for low-cost optical coherence tomography," Biomed. Opt. Express **8**(2), 1110–1121 (2017).
22. J. Xu, C. Zhang, J. Xu, K. K. Y. Wong, and K. K. Tsia, "Megahertz all-optical swept-source optical coherence tomography based on broadband amplified optical time-stretch," Opt. Lett. **39**(3), 622–625 (2014).
23. S. Moon and D. Y. Kim, "Ultra-high-speed optical coherence tomography with a stretched pulse supercontinuum source," Opt. Express **14**(24), 11575–11584 (2006).
24. J. Xi, L. Huo, J. Li, and X. Li, "Generic real-time uniform K-space sampling method for high-speed swept-source optical coherence tomography," Opt. Express **18**(9), 9511–9517 (2010).
25. B. Braaf, K. A. Vermeer, V. A. D. P. Sicam, E. van Zeeburg, J. C. van Meurs, and J. F. de Boer, "Phase-stabilized optical frequency domain imaging at 1-μm for the measurement of blood flow in the human choroid," Opt. Express **19**(21), 20886–20903 (2011).
26. M. Gora, K. Karnowski, M. Szkulmowski, B. J. Kaluzny, R. Huber, A. Kowalczyk, and M. Wojtkowski, "Ultra high-speed swept source OCT imaging of the anterior segment of human eye at 200 kHz with adjustable imaging range," Opt. Express **17**(17), 14880–14894 (2009).
27. S. Kim, P. D. Raphael, J. S. Oghalai, and B. E. Applegate, "High-speed spectral calibration by complex FIR filter in phase-sensitive optical coherence tomography," Biomed. Opt. Express **7**(4), 1430–1444 (2016).
28. B. Vakoc, S. Yun, J. de Boer, G. Tearney, and B. Bouma, "Phase-resolved optical frequency domain imaging," Opt. Express **13**(14), 5483–5493 (2005).
29. W. Choi, B. Potsaid, V. Jayaraman, B. Baumann, I. Grulkowski, J. J. Liu, C. D. Lu, A. E. Cable, D. Huang, J. S. Duker, and J. G. Fujimoto, "Phase-sensitive swept-source optical coherence tomography imaging of the human retina with a vertical cavity surface-emitting laser light source," Opt. Lett. **38**(3), 338–340 (2013).
30. B. Park, M. C. Pierce, B. Cense, S.-H. Yun, M. Mujat, G. Tearney, B. Bouma, and J. de Boer, "Real-time fiber-based multi-functional spectral-domain optical coherence tomography at 1.3 microm," Opt. Express **13**(11), 3931–3944 (2005).
31. M. A. Choma, A. K. Ellerbee, C. Yang, T. L. Creazzo, and J. A. Izatt, "Spectral-domain phase microscopy," Opt. Lett. **30**(10), 1162–1164 (2005).
32. S. Moon, Y. Qu, and Z. Chen, "Characterization of spectral-domain OCT with autocorrelation interference response for axial resolution performance," Opt. Express **26**(6), 7253–7269 (2018).
33. Y. Ling, Y. Gan, X. Yao, and C. P. Hendon, "Phase-noise analysis of swept-source optical coherence tomography systems," Opt. Lett. **42**(7), 1333–1336 (2017).